International Journal of Cardiology 276 (2019) 93–99

Contents lists available at ScienceDirect

International Journal of Cardiology

journal homepage: www.elsevier.com/locate/ijcard

Patient-specific in vivo right ventricle material parameter estimation for patients with tetralogy of Fallot using MRI-based models with different zero-load diastole and systole morphologies

Han Yu [a], Pedro J. del Nido [b], Tal Geva [c], Chun Yang [d], Alexander Tang [c], Zheyang Wu [d], Rahul H. Rathod [c], Xueying Huang [e], Kristen L. Billiar [f], Dalin Tang [a,d,*]

[a] School of Biological Science & Medical Engineering, Southeast University, Nanjing, China
[b] Dept. of Cardiac Surgery, Boston Children's Hospital, Dept of Surgery, Harvard Medical School, Boston, MA, USA
[c] Department of Cardiology, Boston Children's Hospital, Department of Pediatrics, Harvard Medical School, Boston, MA, USA
[d] Mathematical Sciences Department, Worcester Polytechnic Institute, Worcester, MA, USA
[e] School of Mathematical Sciences, Xiamen University, Xiamen, Fujian, China
[f] Department of Biomedical Engineering, Worcester Polytechnic Institute, MA, USA

ARTICLE INFO

Article history:
Received 18 April 2018
Received in revised form 31 July 2018
Accepted 7 September 2018
Available online 10 September 2018

Keywords:
Tetralogy of fallot
Pulmonary valve replacement
Myocardium material
Right ventricle mechanical model

ABSTRACT

Patient-specific in vivo ventricle material parameter determination is important for cardiovascular investigations. A new cardiac magnetic image (CMR)-based modeling approach with different zero-load diastole and systole geometries was adopted to estimate right ventricle material parameter values for healthy and patients with Tetralogy of Fallot (TOF) and seeking potential clinical applications. CMR data were obtained from 6 healthy volunteers and 16 TOF patients with consent obtained. CMR-based RV/LV models were constructed using two zero-load geometries (diastole and systole, 2G model). Material parameter values for begin-filling (BF), end-filling (EF), begin-ejection (BE), and end-ejection (EE) were recorded for analyses. Effective Young's moduli (YM) for fiber direction stress-strain curves were calculated for easy comparisons. The mean EE YM value of TOF patients was 78.6% higher than that of the healthy group (HG). The mean end-ejection YM value from worse-outcome TOF group (WG) post pulmonary valve replacement (PVR) surgery was 59.5% higher than that from the better-outcome TOF group (BG). Using begin-filling YM and end-ejection YM as predictors and the classic logistic regression model to different better-outcome group patients from worse-outcome group patients, the areas under Receiver Operating Characteristic (ROC) curves were found to be 0.797 and 0.883 for begin-filling YM and end-ejection YM, respectively. The sensitivity and specificity 0.761 and 0.755 using end-ejection YM as the predictor. This preliminary study suggests that ventricle material stiffness could be a potential parameter to be used to differentiate BG patients from WG patients with further effort and large-scale patient data validations.

1. Introduction

Tetralogy of Fallot (TOF) is the most common cyanotic congenital heart defect, with an incidence of 32.6 per 100,000 live births [1–3]. The major symptoms of TOF include ventricular septal defect, overriding of the aorta, right ventricular outflow obstruction and right ventricular hypertrophy, which will cause low blood oxygenation resulting in failure to thrive, dyspnea, and cyanosis [3–5]. Corrective surgery aims to completely close the ventricular septal defect and create an unobstructed ventricular outflow tract. The surgery is implemented on the patients in several months after birth. Since the introduction of open-heart surgery, early mortality of TOF patients has steadily decreased to <2%, and approximately 90% of TOF patients are alive at 30 years [6–9]. However, many long time repaired TOF survivors are left with

Abbreviations: BE, begin-ejection; BF, begin-filling; BG, better post-PVR outcome group; CMR, cardiac magnetic resonance; EF, ejection fraction; EDV, End-diastole volume; EE, end-ejection; EF (EF also stands for ejection fraction. We will use full words "end-filling" if confusion arises), end-filling; ESV, End-systole volume; FPR, false positive rate; HG, Healthy human group; LV, left ventricle; PVR, pulmonary valve replacement; ROC, Receiver operating characteristic; RV, right ventricle; RVEF, RV ejection fraction; ΔEF, RV EF change; TOF, tetralogy of Fallot; TPR, true positive rate; WG, worse post-PVR outcome group; YM, Young's moduli/modulus.

* Corresponding author at: Mathematical Sciences Department, Worcester Polytechnic Institute, Worcester, MA 01609, USA.
E-mail addresses: pedro.delnido@cardio.chboston.org (P.J. del Nido), tal.geva@cardio.chboston.org (T. Geva), zheyangwu@WPI.EDU (Z. Wu), rahul.rathod@cardio.chboston.org (R.H. Rathod), xhuang@xmu.edu.cn (X. Huang), kbilliar@WPI.EDU (K.L. Billiar), dtang@wpi.edu (D. Tang).

https://doi.org/10.1016/j.ijcard.2018.09.030
0167-5273/

residual hemodynamic lesions, with severe pulmonary regurgitation (PR), right ventricular (RV) dysfunction, RV overload, RV dilation, decreased exercise tolerance, right heart failure, symptomatic arrhythmias and sudden cardiac death [6,10–12]. The current surgical approach addressing those issues, which includes pulmonary valve replacement/insertion (PVR), has yielded mixed results, with some patients showing improvements, and some others do not [8,13–15]. Identifying risk factors which could differentiate patients with better outcome from those with worse outcome remains to be a challenge to researchers in the field.

Huge effort has been put into developing various innovative surgical options to improve post-PVR outcome [13]. Mathematical, computational, and patient-specific cardiac magnetic resonance (CMR) image-based models were developed to investigate cardiac mechanics and potential clinical applications in the past two decades [16–21]. The early magnetic resonance imaging (MRI)-based ventricle models for mechanical analysis and investigations included Axel et al. [22] and Saber et al. [23]. Several groups investigated myocardium mechanical material properties due to its importance in computational modeling and cardiac function and disease development [24–28]. Sacks et al. and Humphrey et al. reported biaxial mechanical testing results for passive ventricle tissues [24,25]. Holmes et al. indicated that image-based cardiac mechanical models could provide useful information for clinical and surgical applications [26]. Most ventricle models used material properties from existing literature since patient-specific in vivo ventricle material property data is often unavailable and is in general lacking in the current literature.

Echo-based patient-specific models were introduced to estimate in vivo left ventricle material properties with and without infarction [29–31]. In this paper, patient-specific CMR-based models were constructed to quantify RV material properties for healthy volunteers ($n = 6$) and TOF patients ($n = 16$). Differences between healthy and TOF patients and differences between patients with better post-PVR outcome and those with worse outcome were also quantified.

2. Methods

2.1. Data acquisition and 3D geometry reconstruction

CMR data from 6 volunteers and 16 TOF patients before and 6 months after PVR were obtained who were previously enrolled in our RV surgical remodeling trial [14]. The Boston Children's Hospital Committee on Clinical Investigation approved the study. The IRB approval number is: IRB-CRM09-04-0237. Written informed consent was obtained from participants. Data acquisition techniques were previously published and details are omitted here to avoid repetition [19]. Ventricle pressure data were obtained from pre-PVR cardiac catheterization procedures (see Fig. 1). The valve and patch positions were determined with cine MR imaging, flow data, and delayed enhancement CMR to delineate location and extent of scar/patch, and were further verified by the surgeon (PJdN, 30 years of experience) who performed PVR for those patients. Ventricular volume and ejection fraction (EF) were measured by manual tracing of endocardial and epicardial borders on each short-axis steady-state free precession cine slices throughout the entire cardiac cycle. Analyses were performed using commercially available software (QMass, Medis Medical Imaging Systems, Leiden, the Netherlands). Simpson's method was applied to calculate end-diastolic volume (EDV), end-systolic volume (ESV), stroke volume and ejection fraction for analysis.

The 22 cases (6 healthy and 16 repaired TOF patients before PVR, 9 female, average age 36.6) were divided into healthy group (HG), better post-PVR outcome group (BG) and worse post-PVR outcome group (WG) (see Table 1). Selected CMR slices, corresponding segmented contour plots, reconstructed 3D RV/LV geometry with scar, patch and myocardium fiber orientation, and measured ventricle diastole and systole pressure conditions from a TOF patient are given by Fig. 1.

2.2. The pre-shrink process to obtain zero-load diastole and systole geometries

Under in vivo condition, the ventricle is under pressure and its zero-load geometry is unknown. However, our models start from zero-stress geometries (the reference geometries) with zero pressure and zero stress and strain assigned. In reality, it is near impossible to obtain ventricle zero-stress geometry from in vivo CMR data. We used zero-load geometries as approximations to zero-stress geometries. Since zero-stress myocardium sarcomere length shortens and relaxes in ventricle active contraction and relaxation, two different models (diastole and systole models) were constructed to simulate ventricle diastole and systole phases, using different zero-load diastole and systole geometries with corresponding pressure conditions, respectively. Material stiffening and softening were also used during diastole and systole phases corresponding to ventricle relaxation (diastole) and contraction (systole). These models are called 2G models since two zero-load geometries are used [20]. The isovolumic contraction and relaxation phases were skipped in our models since these two phases involve dynamic sarcomere shortening and relaxation which require constant reference coordinate system changes with time that are difficult to implement.

In the model construction process, a pre-shrink process was applied to the in vivo minimum volume ventricular geometry to obtain the two zero-load geometries so that when in vivo pressure was applied, the ventricle would regain its in vivo geometry. Fig. 1 gives the zero-load diastole and systole geometries from one TOF patient. The zero-load systole geometry is smaller reflecting shortened zero-stress sarcomere length. Mass conservative law was observed in the pre-shrink process.

2.3. Nonlinear modified Mooney-Rivlin model used as material models

The nonlinear Mooney-Rivlin model was used to describe the nonlinear anisotropic (myocardium) and isotropic (scar and patch) material properties. The strain

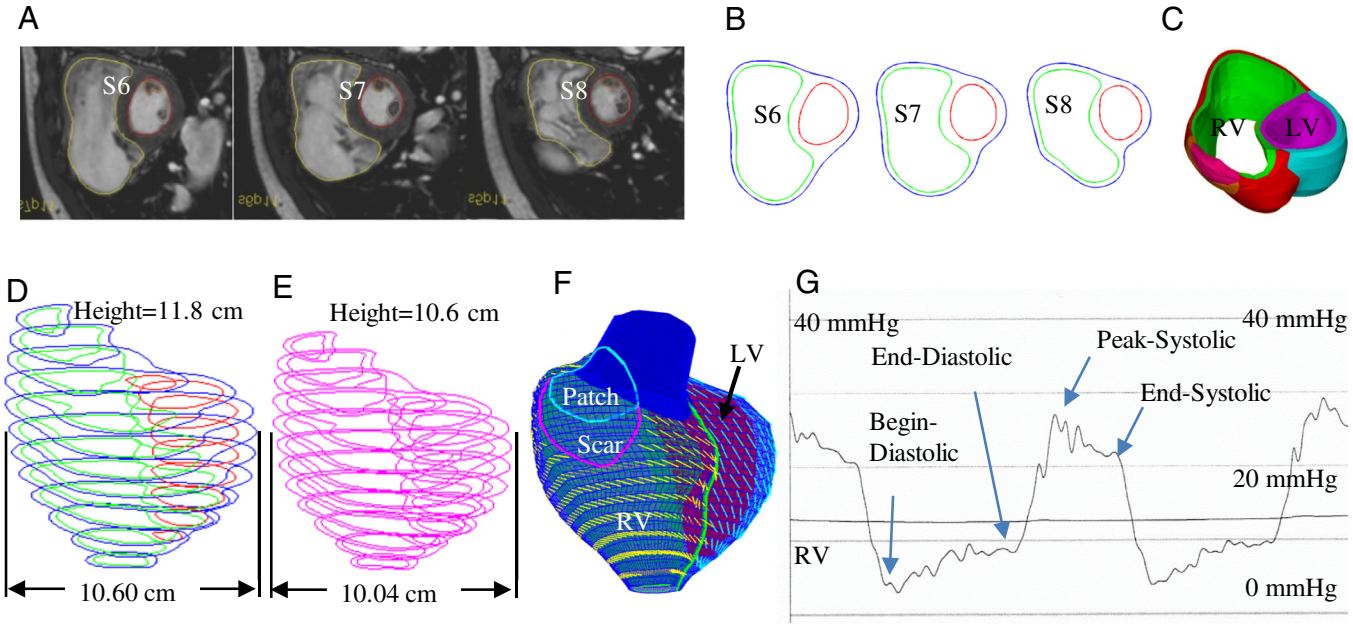

Fig. 1. Illustration of CMR–based model construction process and pressure conditions. A, Selected CMR slices from a patient, end of systole. B, Segmented contours. C, Two-layer structure. D, Zero-load diastole geometry. E, Zero-load systole geometry. F, Model with fiber orientations. G, Recorded RV pressure profile.

Table 1
Demographic and CMR data for healthy human and TOF patients.

Patient no.	Sex	Age (y)	Maximum pressure (mm Hg)	RV EDV (cm^3)	RV ESV (cm^3)	RV EF (%)	ΔEF (%)
Healthy group (HG)							
P1	F	46.7	22	128.4	46.9	63	–
P2	M	23.6	27.9	226.6	105.4	53	–
P3	M	20.8	24	231.7	107.0	54	–
P4	M	19.4	23.8	213.5	94.2	56	–
P5	M	17.7	24.3	233.7	105.5	55	–
P6	M	6.7	24.8	67.6	28.2	58	–
Mean ± SD		22.5 ± 13.2	24.5 ± 1.93	183.6 ± 69.4	81.2 ± 34.6	56.5 ± 3.62	–
Better-outcome patient group (BG)							
P7	M	22.5	31.4	406.9	254.5	37.5	1.4
P8	F	38.5	28	328.8	196.0	40.4	−3.4
P9	M	47.7	31	408.8	254.8	37.7	−2.6
P10	M	50.0	33	364.6	239.5	34.3	−2.9
P11	F	42.0	45	323.3	177.8	45.0	4.0
P12	F	14.3	29	204.0	104.3	48.8	5.6
P13	F	15.3	15	193.7	105.1	45.7	6.6
P14	M	17.0	27	188.3	108.3	42.5	2.0
Mean ± SD		22.2 ± 11.5	29.5 ± 10.7	263.2 ± 97.7	150.0 ± 66.2	43.9 ± 4.22	3.92 ± 2.24
p value[1]		0.572	0.029	0.142	0.02	0.001	
Worse-outcome patient group (WG)							
P15	F	56.9	41	385.1	184.6	52.1	−18.0
P16	M	11.6	36	204.2	121.3	40.6	−8.4
P17	M	43.5	65	665.1	464.0	30.2	−15.2
P18	M	54.1	63	334.8	170.8	49.0	−7.0
P19	F	49.5	52	277.2	151.3	45.4	−5.0
P20	M	17.8	30	365.0	178.0	51.2	−9.5
P21	F	44.6	50	299.0	186.0	37.8	−12.3
P22	F	45.3	49	571.1	371.3	35.0	−13.4
Mean ± SD		41.8 ± 14.4	43.5 ± 13.2	382.2 ± 131	228.9 ± 102	41.2 ± 7.27	−8.88 ± 5.29
p value[2]		0.234	0.004	0.328	0.645	0.574	0.000
p value[3]		0.141	0.000	0.008	0.001	0.001	
p value[4]		0.223	0.003	0.020	0.002	0.001	

F: Female; M: male; EDV: end-diastolic volume; ESV: end-systolic volume; EF: ejection fraction.
[1] p value: comparison between Healthy Group and Better Group.
[2] p value: comparison between Better Group and Worse Group.
[3] p value: comparison between Healthy Group and Worse Group.
[4] p value: comparison between Healthy Humans and TOF Patients.

energy function for the isotropic modified incompressible Mooney-Rivlin model is given by.

$$W = c_1(I_1-3) + c_2(I_2-3) + D_1\left[e^{D_2(I_1-3)}-1\right] \quad (1)$$

where I_1, and I_2 are the first and second strain invariants,

$$I_1 = \sum C_{ii}, I_2 = \frac{1}{2}\left(I_1^2 - C_{ij}C_{ij}\right), \ i,j = 1,2,3 \quad (2)$$

$\boldsymbol{C} = [C_{ij}] = \boldsymbol{X}^T\boldsymbol{X}$ is the right Cauchy-Green deformation tensor. $\boldsymbol{X} = [X_{ij}] = [\partial x_i/\partial a_j]$, where x_i is the current location and a_j is the original location. c_1, c_2, D_1, and D_2 are the material parameters and were chosen to match experimental measurements [32]. The strain energy function for the anisotropic modified Mooney-Rivlin model is given by Tang et al. [19,20,29–31]:

$$W = c_1(I_1-3) + c_2(I_2-3) + D_1\left(e^{D_2(I_1-3)}-1\right) + \frac{K_1}{K_2}\left(e^{K_2(I_4-1)^2}-1\right) \quad (3)$$

where $I_4 = C_{ij}(n_f)_i(n_f)_j$, C_{ij} is the Cauchy-Green deformation tensor, n_f is the fiber direction, K_1 and K_2 are the material parameters. Biaxial test was also performed, indicating that with parameters well chosen, the modified Mooney-Rivlin model could fit the direct measurement of experiment stress-strain data [19,20,33–35].

The orientations of myofibrils cause the myocardial tissue to exhibit mechanical anisotropy [36]. In our 2-layer models, left ventricular (LV) fiber orientation was approximately −60° (relative to circumferential direction) at the epicardium and +80° at the endocardium. RV fiber orientation was set at −45° at the epicardium and +40° at the endocardium [16,35,37] (see Fig. 1(f)).

2.4. Governing equations and boundary conditions

The governing equations for RV/LV models were as follows,

$$\rho v_{i,tt} = \sigma_{ij,j}, \quad i,j = 1,2,3, \quad (4)$$

$$\varepsilon_{ij} = \left(v_{i,j} + v_{j,i} + v_{\alpha,i}v_{\alpha,j}\right)/2, \ \ i,j,\alpha = 1,2,3 \quad (5)$$

$$p|_{RV} = p|_{RV}(t), p|_{LV} = p|_{LV}(t) \quad (6)$$

where $\boldsymbol{\sigma}$ is the stress tensor, ρ is the material density, $\boldsymbol{v}$ is displacement, and $\boldsymbol{\varepsilon}$ is the strain tensor. The normal stress was assumed to be zero on the outer RV/LV surface and equal to the pressure conditions imposed on the inner RV/LV surfaces. Structure-only RV/LV models were used to optimize model computing time. These models provided RV volume, ejection fraction and RV stress/strain values for analysis.

2.5. Solution methods and material stiffness data obtained for comparison analysis

The RV/LV computational models were constructed for the 22 patients and solved by ADINA (ADINA R&D, Watertown, MA, USA) using unstructured finite elements and the Newton- Raphson iteration method. Parameters in the Mooney-Rivlin models were adjusted iteratively until good agreement between the computational and CMR-measured volume data was found (error < 0.2%).

Simulation procedures were continued for 3 periods when differences in the solutions between the last two periods became <0.1%. The solutions for the last period were accepted for analysis.

2.6. Calculation of Young's moduli (YM) and statistical method

Since it is not convenient to compare multiple parameters from the nonlinear Mooney-Rivlin material models, effective YM for the fiber direction stress-strain curves over strain interval [0.0, 0.3] at begin-filling (BF), end-filling (EF), begin-ejection (BE) and end-ejection (EE) were calculated using linear approximation with least square

methods for easy comparisons. The abbreviation EF also stands for ejection fraction. We will clarify if its meaning is not self-clear from the context.

The Wilcoxon rank sum test for unpaired observations was used to compare YM value differences between different groups. The Wilcoxon signed rank test for paired treatments was selected to compare YM differences in a cardiac cycle for the same patient groups. For predicting post-PVR outcome, we applied the logistic regression model:

$$\text{logit}(\Pr(y_i = 1)) = \beta_0 + \beta_1 YM_i \quad (7)$$

where $y_i = 1$ denotes the positive outcome corresponding to better post-PVR outcome and $y_i = 0$ denotes the negative outcome corresponding to worse post-PVR outcome at the i^{th} patient. The YM was used as the predictor to check its prediction accuracy. Both begin-filling YM and end-ejection YM were studied. The gradient descent method was used to obtain the coefficients by the training data, and the obtained logistic regression model was applied as the prediction model into the testing data. For randomly splitting data into training and testing sets, a 5-fold cross-validation procedure was adopted [19,20]. To stabilize the result, the prediction process was repeated 50 times, each with a random partition of training and testing groups. Receiver operating characteristic (ROC) curve together with false positive rate (FPR, specificity) and true positive rate (TPR, sensitivity) were determined to qualify classification efficiency.

3. Results

Table 2 gives a summary of YM values and Fig. 2 provides plots of stress-strain curves for the fiber direction from Mooney-Rivlin models for the 6 healthy volunteers and 16 TOF patients. For the 4 time points from the 2G models, material stiffness at end-filling and end-ejection were the softest and stiffest, respectively. For comparison purpose, results from previous models using one zero-load geometry (called 1G models) were also included in Table 2 and Fig. 2. Patient group comparisons were done using 2G results. Details are given below.

3.1. The TOF patient end-ejection mean YM value was 78.6% higher than that of the healthy group

From the 2G models, the TOF mean end-ejection YM value was 1952 kPa, which is 78.6% higher than that of the healthy group value (1093 kPa, $p = 0.016$). For patient variations, the healthy group end-ejection YM values changed from 797 kPa to 1290 kPa, while the TOF patient end-ejection YM values changed from 759 kPa to 3188 kPa, much greater than the range of the healthy group.

Ventricle material stiffness has large changes in a cardiac cycle due to active contraction and relaxation reflected by YM value changes seen in Table 2. The healthy group mean end-ejection YM value was 1093 kPa, which is 27 times of its end-filling value (40.5 kPa). The mean TOF end-ejection YM value was 1952 kPa, which is about 9 times of its end-filling value (215 kPa). The YM value variations of healthy in a cardiac cycle is much greater than that of the TOF group

Table 2
Young's moduli for 2G models in fiber direction (strain interval [0.0, 0.3]).

Patient	1G models		2G models			
	BF (kPa)	BE (kPa)	BF (kPa)	EF (kPa)	BE (kPa)	EE (kPa)
Healthy group						
P1	910.9	75.9	910.9	15.2	17.5	1062.7
P2	986.8	113.9	986.8	45.5	53.1	1138.6
P3	683.2	75.9	683.1	30.4	38.0	797.0
P4	1070.3	129.0	1070.3	56.9	60.7	1282.9
P5	1062.7	151.8	1062.7	60.7	68.3	1290.4
P6	759.1	75.9	759.1	34.2	35.7	986.8
Mean ± SD	912.2 ± 160.7	103.7 ± 32.7	912.2 ± 160.7	40.5 ± 17.3	45.5 ± 18.7	1093.3 ± 188.1
Better group						
P7	1366.4	835.0	1366.4	303.6	455.5	1783.
P8	1897.7	546.5	1897.7	220.1	265.7	2125.4
P9	1358.8	417.5	1358.8	174.6	189.8	1594.1
P10	1897.7	835.0	1897.7	356.8	379.5	1973.6
P11	1518.2	235.3	1518.2	75.9	87.3	1821.8
P12	683.2	113.9	683.2	41.0	43.3	986.8
P13	607.3	113.9	607.3	38.0	45.5	759.1
P14	645.2	227.7	645.2	83.5	106.3	986.8
Mean ± SD	1244.9 ± 536.8	415.6 ± 297.3	1244.9 ± 536.8	161.7 ± 122.6	196.6 ± 156.6	1503.9 ± 518.8
p value(1)	0.435	0.013	0.435	0.020	0.020	0.281
Worse group						
P15	1373.9	98.7	1373.9	38.0	41.7	1897.7
P16	1670.0	539.0	1670.0	227.7	288.5	2277.3
P17	3036.4	1897.7	3036.4	683.2	873.0	3188.2
P18	1214.5	151.8	1214.5	53.1	64.5	1594.1
P19	1404.3	303.6	1404.3	113.9	144.2	2049.5
P20	2049.5	189.8	2049.5	66.8	72.9	2277.3
P21	2884.5	1100.7	2884.5	432.7	531.4	3112.3
P22	2429.1	1214.5	2429.1	531.4	637.6	2808.6
Mean ± SD	2007.8 ± 708.6	687.0 ± 650.7	2007.8 ± 708.6	268.3 ± 248.9	331.7 ± 313.0	2400.6 ± 579.4
p value(2)	0.049	0.626	0.049	0.524	0.573	0.008
p value(3)	0.001	0.005	0.001	0.013	0.008	0.001
Mean(4) ± SD	1626.3 ± 723.9	551.3 ± 508.4	1626.3 ± 723.9	215.0 ± 197.4	264.2 ± 249.1	1952.3 ± 704.8
p value(5)	0.027	0.004	0.027	0.007	0.006	0.016
Mean(6) ± SD	1431.6 ± 697.4	429.2 ± 457.9	1431.6 ± 697.4	167.4 ± 185.0	204.5 ± 233.1	1718.0 ± 718.7

Notes
[1] p value for comparison between Healthy Group and Better Group.
[2] p value for comparison between Better Group and Worse Group.
[3] p value for comparison between Healthy Group and Worse Group.
[4] Mean and SD for the whole TOG group; SD: Standard Deviation.
[5] p value for comparison between Healthy Humans and TOF Patients.
[6] Mean and SD for all 22 cases studies (6 HG + 16 TOG).

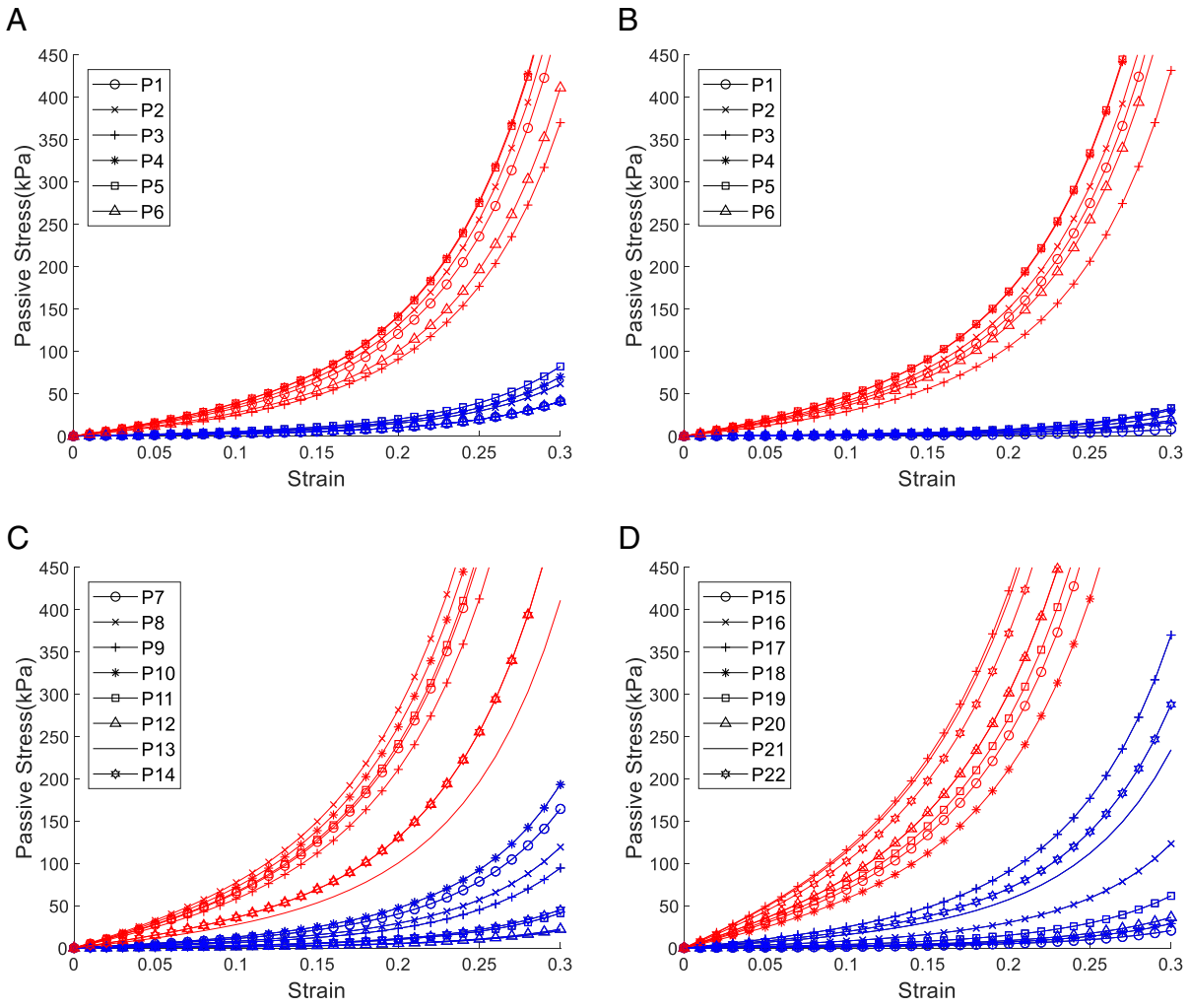

Fig. 2. Plots of stress-strain curves from Mooney-Rinlin models in fiber direction. A, 1G model curves from healthy group. B, 2G model curves from healthy group. C, 2G model curves from better outcome group. D, 2G model curves from worse outcome group. Red: stress-strain curves at end-ejection. Blue: Red: stress-strain curves at end-filling.

indicates that the contractibility of healthy ventricles is better than the TOF ventricles.

3.2. Mean end-ejection YM values from worse-outcome group was 59.5% higher than that from the better-outcome group

The mean end-ejection YM values of the worse-outcome group was 2400 kPa, which is 59.5% higher than that of the better-outcome group value (1504 kPa, $p = 0.008$). The mean begin-filling YM of worse-outcome group was 61.3% higher than that of better-outcome group (2008 kPa vs. 1245 kPa, $p = 0.049$).

3.3. Using ventricle material parameters to differentiate BG and WG patients

Using begin-filling YM and end-ejection YM as predictors and the predictive model (7) to different better-outcome group patients from worse-outcome group patients, the areas under Receiver Operating Characteristic (ROC) curves were found to be 0.797 and 0.883 for begin-filling YM and end-ejection YM, respectively. The sensitivity and specificity were 0.723 and 0.594 using begin-filling YM as the predictor, and 0.761 and 0.755 using end-ejection YM as the predictor. No statistically significant differences were found for end-filling YM and begin-ejection YM values between better-outcome group and worse-outcome group.

4. Discussion

4.1. Significant improvement of the 2G models over models using one zero-load geometry

Most ventricle models (including our own previous models) used one zero-load geometry (1G model) since it is computationally very challenging to constantly change model reference frame. 2G models improved over 1G models by using different zero-load diastole and systole geometries with corresponding correct end-diastole and end-systole pressure conditions. By using different zero-load geometries for diastole and systole phases, the 2G models provide better approximations for zero-stress sarcomere length and the stress/strain calculations are based on more accurate reference frames for diastole and systole phases, respectively. Using correct reference frame is a basic requirement for correct stress/strain calculations. Detailed comparison between 1G and 2G models is given in the appendix for interested readers.

4.2. Quantification of patient-specific ventricle material properties for healthy and TOF patients

Our initial intent was to quantify ventricle material properties for the healthy and TOF patients and investigate their differences. To the best of our knowledge, the results presented in the paper should be

the first publication of its kind. Clearly, TOF patient ventricle materials were much stiffer than that of healthy group. We also demonstrated that ventricle material stiffness varies greatly from begin-filling to end-filling and from begin-ejection to end-ejection. With the use of different zero-load geometries, we were able to quantify ventricle stiffness variations in diastole and systole phases separately.

It should be noted that ventricle stiffness variation is closely linked to its contractibility and how the model handles active contraction. Results presented in this paper should be interpreted with our model assumptions, i.e., different zero-load geometries were used for diastole and systole phases, and material stiffness was adjusted softer and stiffer to reflect ventricle relaxation and stiffening, respectively.

It is natural to think about getting direct measurements as validation of our modeling results. In a way, matching CMR-measured ventricle volume data for all 30 time points in a cardiac cycle can be considered as validation of our models and model predictions. Other than that, direct measurement of material properties under in vivo condition is nearly impossible, especially when zero-stress reference data is needed. Those remain as challenges for the research community.

As an effort in seeking the ground truth and supporting data for human ventricle material properties, ex vivo biaxial mechanical testing using right ventricle tissue from a human cadaver was performed using established methods and the recorded data were plotted in Fig. 3 [20,24,33]. The corresponding fiber-direction and cross-fiber direction YM values and the end-ejection YM values from our models for the 6 healthy volunteers are given in Table 3. The ex vivo data and the modeling results are in good agreement. Considering the differences between in vivo and ex vivo material properties and the active contraction/relaxation handling in our models, and considering that the ex vivo sample were in contracted stage corresponding to our BF and EE data, this is a reasonable support for our findings.

4.3. Clinical usefulness of our stiffness findings

Significant differences of RV material stiffness were found between TOF group and healthy group. We also found statistically significant differences in RV material stiffness between TOF BG and WG patients at begin-filling and end-ejection. These differences could serve as basis for possible predictive methods to differentiate BG patients from WG patients and innovative surgical procedures leading to improved post-PVR outcome by modifying ventricle and patch material properties.

4.4. Limitations

Some limitations of our models are acknowledged here: a) direct measurements of pre-shrink ratios and zero-stress sarcomere fiber contraction rate were not available and existing literature were used [17,24]. b) fluid-structure interaction and valve mechanics were not included; c) patient-specific ventricle fiber orientations were not available and data from the existing literature were used [16,35]; d) small sample size is a limitation. Both getting patient data with follow-up and model construction take a long time (each model takes at least 2–4 weeks to construct and adjust; each patient needs practically 3 models: 1G, 2G systole and 2G diastole). Adding more patients will be our future effort.

Acknowledgement and funding

This research was supported in part by NIH/NHLBI R01 HL089269, National Science Foundation of China 11672001 and 81571691.

Conflict of interest

None.

Appendix A. Comparison between 2G models and models using one zero-load geometry (1G model)

In our previous publications [20] (as well as in most ventricle papers by other researchers), models were constructed using one zero-load ventricle geometries (1G). Our previous 1G models used zero-load geometries which were the same as our diastole zero-load geometries of our 2G models. Those 1G models had their minimum ventricle volume under minimum pressure. This state was defined as both begin-filling and end-ejection states. Similarly, their maximum volume was under maximum pressure. This state was defined as both end-filling and begin-ejection states [20].

For 1G models, not only the zero-stress sarcomere length differences were ignored, pressure conditions at end-filling (which is not equal to maximum pressure) and end-ejection (which is not equal to minimum pressure either) were also ignored. Because of that, 1G models have only begin-filling and begin-ejection results and are not able to provide accurate end-filling and end-ejection results. 1G begin-filling stress/strain were taken as end-ejection (end-systole) results, and 1G being-ejection results was taken as end-filling (end-diastole) results as well. Those are often confusing since end-systole and end-diastole are routinely used in the clinical research community while 1G models really could not provide those results.

2G models improved over 1G models by using different zero-load diastole and systole geometries with corresponding correct end-diastole and end-systole pressure conditions. By using different zero-load geometries for diastole and systole phases, the 2G models provide better approximations for zero-stress sarcomere length and the stress/strain calculations are based on more accurate reference frames for diastole and systole phases, respectively. Using correct reference frame is a basic requirement for correct stress/strain calculations.

Comparing 1G and 2G models, 1G begin-ejection mean YM value was 429 kPa, which is 109% higher than that (205 kPa) from 2G model ($p = 0.00004$). 1G mean end-ejection (which is the same as begin-filling for 1G) YM value was 1432 kPa, 16.7% lower than that (1718 kPa) from 2G model ($p = 0.00004$). That is due to different zero-load systole geometry and end-ejection pressure conditions. 2G mean end-filling YM value was 167.0 kPa, which is only 39% of 1G begin-ejection (which is the same as end-filling for 1G model) YM value 429.2 kPa ($p = 0.00004$). That is because end-filling pressure condition in 2G model is lower than maximum pressure that 1G model used as end filling/being-ejection pressure conditions.

Appendix B. Supplementary data

Supplementary data to this article can be found online at https://doi.org/10.1016/j.ijcard.2018.09.030.

References

[1] A.L. Christopher, Epidemiology of cardiovascular malformations: prevalence and risk factors, Am. J. Med. Genet. C: Semin. Med. Genet. 97 (2000) 319–325.
[2] I.E.H. Julien, K. Samuel, The incidence of congenital heart disease, J. Am. Coll. Cardiol. 39 (2002) 1890–1900.
[3] W.W. Lai, L.M. Luc, M.S. Cohen, T. Geva, Echocardiography in Pediatric and Congenital Heart Disease: From Fetus to Adult, John Wiley & Sons, 2015.
[4] R.W. Sprengers, A.A.W. Roest, L.J.M. Kroft, Tetralogy of Fallot, Medical Radiology, Springer, Berlin, Heidelberg, 2017.
[5] C. Apitz, D.W. Gary, N.R. Andrew, Tetralogy of fallot, Lancet 374 (2009) 1462–1471.
[6] T. Geva, M. Sandweiss Bryan, K. Gauvreau, J.E. Lock, A.J. Powell, Factors associated with impaired clinical status in long-term survivors of tetralogy of Fallot repair evaluated by magnetic resonance imaging, J. Am. Coll. Cardiol. (2004) 431068–431074.
[7] E.A. Bacha, A.M. Scheule, D. Zurakowski, L.C. Erickson, J. Hung, P. Lang, J.E. Mayer Jr., Pedro J. del Nido, Richard A. Jonas, Long-term results after early primary repair of tetralogy of Fallot, J. Thorac. Cardiovasc. Surg. 122 (2001) 154–161.
[8] G. Nollert, T. Fischlein, S. Bouterwek, C. Boehmer, W. Klinner, B. Reichart, Long-term survival in patients with repair of tetralogy of Fallot: 36-year follow-up of 490 survivors of the first year after surgical repair, J. Am. Coll. Cardiol. 30 (1997) 1374–1383.
[9] J.G. Murphy, B.J. Gersh, D.D. Mair, V. Fuster, M.D. McGoon, D.M. Ilstrup, D.C. McGoon, J.W. Kirklin, Gordon K. Danielson, Long-term outcome in patients undergoing surgical repair of tetralogy of Fallot, N. Engl. J. Med. 329 (1993) 593–599.

[10] Y.Y. Kim, Emily Rl, Approach to residual pulmonary valve dysfunction in adults with repaired tetralogy of Fallot, Heart 102 (2016) 1520–1526.
[11] M. Greutmann, Tetralogy of Fallot, pulmonary valve replacement, and right ventricular volumes: are we chasing the right target? Eur. Heart J. 37 (2015) 836–839.
[12] Michael A. Gatzoulis, S. Balaji, S.A. Webber, S.C. Siu, J.S. Hokanson, C. Poile, M. Rosenthal, M. Nakazawa, J.H. Moller, P.C. Gillette, G.D. Webb, A.N. Redington, Risk factors for arrhythmia and sudden cardiac death late after repair of tetralogy of Fallot: a multicentre study, Lancet 356 (2000) 975–981.
[13] P.J. Del Nido, Surgical management of right ventricular dysfunction late after repair of tetralogy of Fallot: right ventricular remodeling surgery, Semin. Thorac. Cardiovasc. Surg. Pediatr. Card. Surg. Annu. 9 (2006) 29–34.
[14] T. Geva, K. Gauvreau, A.J. Powell, F. Cecchin, J. Rhodes, J. Geva, P. del Nido, Randomized trial of pulmonary valve replacement with and without right ventricular remodeling surgery, Circulation 122 (2010) S201–S208.
[15] E.D. McKenzie, M.S. Khan, T.W. Dietzman, F.A. Guzm An-Pruneda, A.X. Samayoa, A. Liou, J.S. Heinle, C.D. Fraser Jr., Surgical pulmonary valve replacement: a benchmark for outcomes comparisons, J. Thorac. Cardiovasc. Surg. 148 (2014) 1450–1453.
[16] P.J. Hunter, A.J. Pullan, B.H. Smaill, Modeling total heart function, Annu. Rev. Biomed. Eng. 5 (2003) 147–177.
[17] A.D. McCulloch, L. Waldman, J. Rogers, J.M. Guccione, Large-scale finite element analysis of the beating heart, Crit. Rev. Biomed. Eng. 20 (1992) 427–449.
[18] G.M. Fomovsky, J.R. Macadangdang, G. Ailawadi, J.W. Holmes, Model-based design of mechanical therapies for myocardial infarction, J. Cardiovasc. Transl. Res. 4 (2011) 82–91, https://doi.org/10.1007/s12265-010-9241-3.
[19] D. Tang, P.J. Del Nido, C. Yang, H. Zuo, X. Huang, H. Rathod Rahul, Gooty Vasu, Tang Alexander, Wu Zheyang, L. Billiar Kristen, Geva Tal, Patient-specific MRI-based right ventricle models using different zero-load diastole and systole geometries for better cardiac stress and strain calculations and pulmonary valve replacement surgical outcome predictions, PLoS One 11 (9) (2016), e0162986. https://doi.org/10.1371/journal.pone.0162986.
[20] T. Dalin, Y. Chun, J. del Nido Pedro, Z. Heng, Rahul H. Rathod, H. Xueying, H. Vasu, T. Alexander, Kristen L. Billiar, W. Zheyang, T. Geva, Mechanical stress is associated with right ventricular response to pulmonary valve replacement in patients with repaired tetralogy of Fallot mechanical stress, J. Thorac. Cardiovasc. Surg. 151 (2015) 687–694.
[21] K.D. Costa, P.J. Hunter, J.M. Rogers, J.M. Guccione, L.K. Waldman, A.D. McCulloch, A three-dimensional finite element method for large elastic deformations of ventricular myocardium: I—cylindrical and spherical polar coordinates, J. Biomech. Eng. 118 (1996) 452–463.
[22] L. Axel, Biomechanical dynamics of the heart with MRI, Annu. Rev. Biomed. Eng. 4 (2000) 321–347.
[23] N.R. Saber, A.D. Gosman, N.B. Wood, P.J. Kilner, C.L. Charrier, D.N. Firman, Computational flow modeling of the left ventricle based on in vivo MRI data: initial experience, Ann. Biomed. Eng. 29 (2001) 275–283.
[24] M.S. Sacks, C.J. Chuong, Biaxial mechanical properties of passive right ventricular free wall myocardium, J. Biomech. Eng. 115 (1993) 202–205.
[25] J.D. Humphrey, R.K. Strumpf, F.C. Yin, Biaxial mechanical behavior of excised ventricular epicardium, Am. J. Phys. 259 (1990) H101–H108.
[26] J.W. Holmes, K.D. Costa, Imaging cardiac mechanics: what information do we need to extract from cardiac images? Conf. Proc. IEEE Eng. Med. Biol. Soc. 1 (2006) 1545–1547.
[27] Y. Gan, Q. Chen, S. Zhang, S. Ju, Z.Y. Li, MRI-based strain and strain rate analysis of left ventricle: a modified hierarchical transformation model, Biomed. Eng. Online 14 (2005) S1–S9.
[28] L. Asner, M. Hadjicharalambous, R. Chabiniok, D. Peresutti, E. Sammut, J. Wong, G. Carr-White, P. Chowienczyk, J. Lee, A. King, N. Smith, R. Razavi, D. Nordsletten, Estimation of passive and active properties in the human heart using 3D tagged MRI, Biomech. Model. Mechanobiol. 15 (2016) 1121–p1139.
[29] R. Fan, D. Tang, J. Yao, C. Yang, D. Xu, 3D echo-based patient-specific computational left ventricle models to quantify material properties and stress/strain differences between ventricles with and without infarct, Comput. Model. Eng. Sci. 99 (6) (2014) 491–508.
[30] L. Fan, J. Yao, C. Yang, Z. Wu, D. Xu, D. Tang, Material stiffness parameters as potential predictors of presence of left ventricle myocardial infarction: 3D echo-based computational modeling study, Biomed. Eng. Online 15 (2016 Apr 5) 34.
[31] L. Fan, J. Yao, C. Yang, Xu Di, Tang Dalin, Using 3D Echo-based modeling to quantify in vivo ventricle material properties: a multi-patient study, Procedia Eng. 126 (2015) 446–450.
[32] T. Dalin, Y. Chun, T. Geva, G. Gaudette, P.J. Del Nido, Multi-physics MRI-based two-layer fluid–structure interaction anisotropic models of human right and left ventricles with different patch materials: cardiac function assessment and mechanical stress analysis, Comput. Struct. 89 (11−12) (2011 Jun) 1059–1068.
[33] K.L. Billiar, M.S. Sacks, Biaxial mechanical properties of the natural and glutaraldehyde treated aortic valve cusp—part I: experimental results, J. Biomech. Eng. (2000) 12223–12230.
[34] Jay D. Humphrey, Cardiovascular Solid Mechanics: Cells, Tissues, and Organs, Springer Science & Business Media, 2013.
[35] Damian Sanchez-Quintana, Robert H. Anderson, Siew Yen Ho, Ventricular myoarchitecture in tetralogy of Fallot, Heart 17 (1996) 280–286.
[36] P.H.M. Bovendeerd, T. Arts, J.M. Huyghe, D.H. van Campen, R.S. Renemane, et al., Dependence of local left ventricular wall mechanics on myocardial fiber orientation: a model study, J. Biomech. 25 (1992) 1129–1140.
[37] C. Yang, D. Tang, T. Geva, Rathod Rahul, Gooty Vasu, Tang Alexander, Yamauchi Haruo, J. del Nido Pedro, Gaudette Glenn, L. Billiar Kristen, Mehmet H. Kural, Using contracting band to improve right ventricle ejection fraction for patients with repaired tetralogy of Fallot: a modeling study using patient-specific CMR-based 2-layer anisotropic models of human right and left ventricles, J. Thorac. Cardiovasc. Surg. 145 (2013) 285–293.